# ARTICLES

# NUMERICAL SIMULATION OF HYDROCYCLONES FOR CELL SEPARATION

R. A. MEDRONHO[1], J. SCHUETZE[2] and W.-D. DECKWER[3]

[1] *Escola de Química, Univ. Federal do Rio de Janeiro, CT, Bl. E, 21949-900 Rio de Janeiro-RJ, Brazil*
*medronho@ufrj.br*
[2] *Fluent Germany, Hindenburgstrasse 36, D-64295 Darmstadt, Germany*
*jos@fluent.de*
[3] *Technische Universität Braunschweig, GBF-German Research Centre for Biotechnology-TU-BCE, Mascheroder Weg 1, D-38124 Braunschweig, Germany*
*wdd@gbf.de*

*Abstract* — **Numerical simulation of hydrocyclones aiming at investigating the separation of microorganisms and mammalian cells was performed using Computational Fluid Dynamics (CFD). The turbulence model used in the 2d-axisymmetric calculations was the Reynolds Stress Model (RSM), in order to take into account the high swirl effects that occur in this type of equipment, which induce anisotropic turbulence. The Volume of Fluid Model (VOF) was used to account for the gas/liquid interface. In all calculations, a cylindrical air core, running the whole length of the cyclone, appeared naturally as a consequence of a low pressure region that developed along the central axis. The separation of *Escherichia coli*, *Saccharomyces cerevisiae* and mammalian cells (BHK-21) using Bradley hydrocyclones was studied. According to the present work, Bradley hydrocyclones with diameters down to 10 mm cannot efficiently separate microorganisms, but the separation of mammalian cells with predicted efficiencies as high as 90% can be achieved.**

*Keywords* — **CFD, hydrocyclones, separation, microorganisms, mammalian cells**

## I. INTRODUCTION

Hydrocyclones are very simple devices (Fig. 1). In spite of this, research work is still in progress aiming at understanding the complex flow inside this apparatus or at developing new applications.

Regarding flow field, the high swirl effects that occur in hydrocyclones induce anisotropic turbulence, and this is the reason why the $k$-$\varepsilon$ turbulence model is not capable of properly describing the flow in hydrocyclones (He *et al.*, 1999).

Regarding new applications, the use of hydrocyclones for yeast separation either from fermentation broths or from yeast-water suspensions have being investigated by some authors (Rickwood *et al.*, 1992, Yuan *et al.*, 1996a and 1996b, and Cilliers and Harrison, 1997). Even using hydrocyclones as small as 10 mm diameter, these authors could not obtain high separation efficiencies coupled with high underflow concentrations.

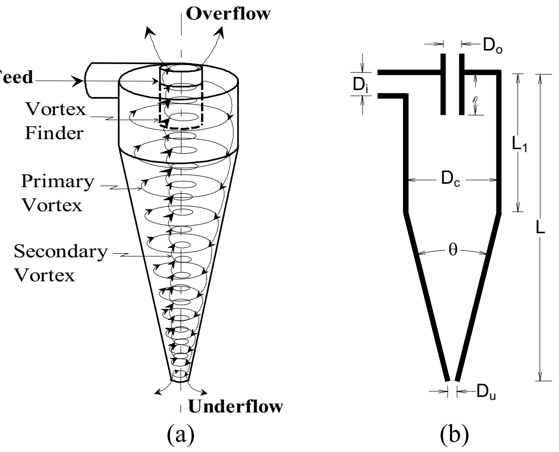


Figure 1. Perspective view of a hydrocyclone showing the fluid flow inside the equipment (a) and a schematic view showing its geometrical variables (b) whose definitions can be found in the item III.A.

A possible new application of hydrocyclones is their use in perfusion culture of mammalian cells. Cell retention in perfusion cultures is normally performed using centrifugation, cross flow microfiltration, spin-filtration, gravitational sedimentation, and ultrasonic separation. Unfortunately, all of these separation processes have specific problems (Castilho and Medronho, 2002). The use of hydrocyclones would increase process reliability, since their maintenance are virtually non-existent, and their service lifetime for this application would be extremely large.

The aim of the present work is to investigate, through the use of computational fluid dynamics (CFD), if hydrocyclones are capable of separating micro-organisms and mammalian cells from a culture medium.

## II. MATHEMATICAL MODELS

### A. The Reynolds Stress Model (RSM)

Equations (1) and (2) are the time-smoothed equations of continuity and momentum transport, respectively (Bird *et al.*, 2001; Launder, 1989).

$$\frac{\partial \rho}{\partial t}+\frac{\partial}{\partial x_i}(\rho U_i)=0 \ , \qquad (1)$$

$$\rho\frac{DU_i}{Dt}=-\frac{\partial p}{\partial x_i}+\frac{\partial}{\partial x_j}\left[\mu\left(\frac{\partial U_i}{\partial x_j}+\frac{\partial U_j}{\partial x_i}\right)\right]+ \\ +\frac{\partial}{\partial x_j}\left(-\rho\overline{u_i u_j}\right)+\rho g_i \ , \qquad (2)$$

where $\rho$ and $\mu$ are the density and viscosity of the liquid, $U_i$ and $u_i$ are the $x_i$ components of the mean fluid velocity and the fluctuating fluid velocity, $p$ is pressure, $g$ is gravity acceleration, and $\rho\overline{u_i u_j}$ are the components of the turbulent moment flux, known as "Reynolds stresses".

A model for the Reynolds stresses is then needed in order to close Eqn. (2). The $k$-$\varepsilon$ model is widely used for this purpose. The problem with this model is that it assumes isotropic turbulence and this condition appears not to hold for the flow inside a hydrocyclone. The RSM abandons the condition of isotropic eddy-viscosity hypothesis and closes the Reynolds-averaged Navier-Stokes equation by solving transport equations for the individual Reynolds stresses, together with an equation for the turbulence energy dissipation rate $\varepsilon$. This means that 4 additional transport equations are required for simple two-dimensional flow calculations, and 7 for two-dimensional flows with swirl, as well as three-dimensional flows (Fluent, 1998). The RSM deals with the effects of streamline curvature, swirl, and rapid changes in the strain rate in a more rigorous manner than the $k$-$\varepsilon$ model does. Therefore it has more potential to give good predictions for the complex flow field inside a hydrocyclone. Since the RSM is a more complex model, it requires on average 50-60% more CPU time per iteration and 15-20% more memory than the k-ε model (Fluent, 1998).

For a turbulent flow, Eqn. (3) can describe the transport of the Reynolds stress tensor (Launder, 1989; Fluent, 1998).

$$\frac{\partial}{\partial t}\left(\rho\overline{u_i u_j}\right)+C_{ij}=D_{ij}^T+D_{ij}^L+P_{ij}+G_{ij}+\phi_{ij}+\varepsilon_{ij}+F_{ij} \ , \qquad (3)$$

where $C_{ij}$ is convection, $D_{ij}^T$ is turbulent diffusion, $D_{ij}^L$ is molecular diffusion, $P_{ij}$ is stress production, $G_{ij}$ is buoyancy production, $\phi_{ij}$ is pressure strain, $\varepsilon_{ij}$ is dissipation, and $F_{ij}$ is production by system rotation. These quantities are given by Eqns. (4) to (11), respectively.

$$C_{ij}=\frac{\partial}{\partial x_k}\left(\rho U_k\overline{u_i u_j}\right) \ , \qquad (4)$$

$$D_{ij}^T=-\frac{\partial}{\partial x_k}\left[\rho\overline{u_i u_j u_k}+\overline{p\left(\delta_{kj}u_i+\delta_{ik}u_j\right)}\right] , \qquad (5)$$

$$D_{ij}^L=\frac{\partial}{\partial x_k}\left[\mu\frac{\partial}{\partial x_k}\overline{u_i u_j}\right] , \qquad (6)$$

$$P_{ij}=-\rho\left(\overline{u_i u_k}\frac{\partial U_j}{\partial x_k}+\overline{u_j u_k}\frac{\partial U_i}{\partial x_k}\right) \ , \qquad (7)$$

$$G_{ij}=\left(\overline{f_i u_j}+\overline{f_j u_i}\right) \ , \qquad (8)$$

$$\phi_{ij}=\overline{p\left(\frac{\partial u_i}{\partial x_j}+\frac{\partial u_j}{\partial x_i}\right)} \ , \qquad (9)$$

$$\varepsilon_{ij}=-2\mu\overline{\frac{\partial u_i}{\partial x_k}\frac{\partial u_j}{\partial x_k}} \ , \qquad (10)$$

$$F_{ij}=-2\rho\Omega_k\left(\overline{u_j u_m}\varepsilon_{ikm}+\overline{u_i u_m}\varepsilon_{jkm}\right) . \qquad (11)$$

### B. The Two-Layer Zonal Model

At walls, the momentum exchange between the moving fluid and the adjacent wall surface may be described. using an empirical dimensionless formulation ("wall function"). Although this approach saves computational resources, for strongly swirling flows like those existing inside hydrocyclones, resolving the viscosity affected near-wall region in a fine near-wall mesh is a vital prerequisite for accurate fluid flow simulations.

In the two-layer zonal model, the flow domain is divided in two parts. The inner part (next to the wall) includes the laminar sublayer and the transition region, and the outer part contains the fully turbulent flow. In the latter, the flow can be resolved using an appropriate turbulence model as the Reynolds stress model. To resolve the former, the Kolmogorov-Prandtl model of turbulence, as formulated by Wolfshtein (1969), can be used. This author proposed the following equations for the eddy viscosity $\mu_t$ and the energy dissipation rate $\varepsilon$:

$$\mu_t=C_\mu\rho\ k^{1/2}\ell_\mu \ , \qquad (12)$$

$$\varepsilon=\frac{k^{3/2}}{\ell_\varepsilon} \ , \qquad (13)$$

where $C_\mu$ is an empirical constant, and $\ell_\mu$ and $\ell_\varepsilon$ are the characteristic length scales of turbulent viscosity and energy dissipation, respectively (Eqns. 14 and 15).

$$\ell_\mu=c_\ell y\left[1-\exp\left(-\frac{\mathrm{Re}_y}{A_\mu}\right)\right] , \qquad (14)$$

$$\ell_\varepsilon=c_\ell y\left[1-\exp\left(-\frac{\mathrm{Re}_y}{A_\varepsilon}\right)\right] , \qquad (15)$$

where $c_\ell$, $A_\mu$, and $A_\varepsilon$ are constants, $y$ is the normal distance from the wall at the cell centre, and $Re_y$ is the turbulent Reynolds number, given by:

$$\mathrm{Re}_y = \frac{y\, k^{1/2} \rho}{\mu} \ . \quad (16)$$

### C. The Volume of Fluid Model (VOF)

The VOF model is a physically rigorous yet efficient grid technique for numerically treating free boundaries between immiscible fluid phases. It uses a function $F$ defined in such a way that its value is unity at any point occupied by one of the fluids and zero otherwise. The mean value of $F$ in a computational cell represents the fractional volume of the cell occupied by this fluid. $F$ values between zero and one indicate that the computational cell must contain an interface (Hirt and Nichols, 1981).

The VOF model solves a single set of momentum equations that are shared by the fluid phases, and the volume fraction of each of the fluids in each computational cell is tracked throughout the domain as a separate conserved quantity. The time dependent transport of $F$ is governed by the following equation:

$$\frac{\partial F}{\partial t} + U_i \frac{\partial F}{\partial x_i} = 0 \ . \quad (17)$$

The fields for all variables and properties are shared by the phases, and represent volume-averaged values in computational cells that contain fractional volumes of more than one fluid phase. For instance, in a multi-phase system the volume-fraction-averaged viscosity in each cell is given by:

$$\mu = \sum_i \overline{F_i} \mu_i \ , \quad (18)$$

where $\overline{F_i}$ is the fractional volume of the cell occupied by fluid i, and $\sum_i \overline{F_i} = 1$.

## III. MATERIALS AND METHODS

### A. The Hydrocyclone, the grid, and the models

Numerical simulations were performed using FLUENT 5.1, a CFD tool from Fluent Inc. The simulated hydrocyclone geometry obeys Bradley's recommended proportions (Bradley, 1965), and its internal dimensions (see Fig. 1b) are $D_c$ = 10.0 mm, $D_i$ = 1.4 mm, $D_o$ = 2.0 mm, and $D_u$ = 1.0 mm for the cylindrical part, inlet, overflow and underflow diameters, respectively; $\ell$ = 3.3 mm, $L_1$ = 5.0 mm, and L = 62.1 mm as vortex finder, cylindrical part, and hydrocyclone lengths, respectively; and $\theta$ = 9° as cone angle. Three two-dimensional grids representing the Bradley hydrocyclone were built with 42295, 68271 and 80116 quadrilateral cells, respectively. Any further increase in cell number did not result in any change in the predicted velocity profiles, indicating that the finest grid was sufficiently fine for mesh-independent flow predictions.

The Reynolds stress turbulence model (RSM) was used to calculate the axisymmetric swirling flow. The volume of fluid (VOF) model was employed to predict the gas/liquid interface, and the two-layer zonal model was used to resolve the viscosity-affected near-wall region of the turbulent flow, with the constants suggested by Chen and Patel (1988):

$$c_\ell = \kappa C_\mu^{-3/4}\ , \quad A_\mu = 70, \quad A_\varepsilon = 2c_\ell\ , \quad C_\mu = 0.09\ . \quad (19)$$

The partial differential equations for mass conservation and the transport of momentum, Reynolds stresses, and turbulent energy dissipation rate ($\varepsilon$) were solved using FLUENT's segregated solver. This is based on the finite-volume method, which turns the differential formulation of all conservation equations into a control-volume based balancing of diffusive and advective fluxes. The latter are directly driven by fluid flow, while the former are intensified by turbulence as described by the applied turbulence model. Velocity components in the axial, radial, and circunferential directions were treated. As all variation of the flow field in circunferential direction was neglected, the simulation could be performed in two dimensions. The solver accounts for all additional terms resulting from the projection of an axisymmetric geometry and flow field into two dimensions.

All simulations were performed in a time-independent manner (steady state assumption). Density and dynamic (laminar) viscosity of the liquid were assumed to be constant, which corresponds to an isothermal approach. Pressure-velocity coupling between continuity and momentum equations was achieved using the *"semi-implicit method for pressure linked equations"*, known as SIMPLE-algorithm (Patankar and Spalding, 1972; Vandoormaal and Raithby, 1984). For pressure discretisation, the *"pressure staggering option"* (PRESTO) scheme was applied. This is a numerical approach that resembles the *"staggered grid method",* described by Patankar (1980). It is particularly suited for the simulation of flow fields involving steep pressure gradients (Fluent, 1998). For the discretisation of all other conservation equations, upwind discretisation was used.

The assumption of a two-dimensional axisymmetric swirling flow implies that the feed has to be equally distributed at the suspension entrance. As used by other authors (He *et al.*, 1999; Hsieh and Rajamani, 1991; Hargeaves and Silvester, 1990; Brayshaw, 1990), a full 360° inlet ring was assumed in the simulations. It is assumed that the fluid entering a hydrocyclone through a tangential inlet pipe quickly distributes itself around the cylindrical section. Therefore, the 360° inlet ring is expected to be a good approximation of this condition (Hsieh and Rajamani, 1991). It allows otherwise accurate simulations in fine two-dimensional grids. The vastly increasing demand in computer memory and time for three-dimensional simulations would enforce the use of much coarser meshes, which eventually would not allow any mesh-independent fluid flow simulation.

**B. The Boundary Conditions**

Uniform velocity boundary conditions were used at the inlet, based on a flow rate of 28 $cm^3\ s^{-1}$. This flow rate was chosen because it lies approximately in the middle of the usual flow rate range quoted in the literature for 10 mm hydrocyclones. The inlet radial velocity was obtained dividing the flow rate by the area of the 360° inlet ring; the swirl velocity at the inlet was assumed to be the average velocity at the actual inlet pipe, and the inlet axial velocity was assumed to be zero. Uniform turbulent kinetic energy $k$ and turbulent dissipation rate $\varepsilon$ were calculated at the inlet using Eqns. (20) and (21) (Fluent, 1998).

$$k = 1.5\left(U_{inlet} I\right)^2 \ , \qquad (20)$$

$$\varepsilon = \frac{C_\mu^{0.75} k^{1.5}}{\ell} \ , \qquad (21)$$

where $U_{\text{inlet}}$ is the average fluid velocity at the inlet, $I$ is the turbulence intensity given by Eqn. (22), and $\ell$ is the turbulence length scale ($\ell$ was assumed to be 7% of the inlet diameter $D_i$, which is approximately the maximum value of the turbulence length scale in fully-developed turbulent flow in pipes).

$$I = 0.16\left(\frac{D_i U_{inlet} \rho}{\mu}\right)^{-1/8} , \qquad (22)$$

where the quantity between brackets is the Reynolds number based on $D_i$ and the average fluid velocity at the inlet $U_{\text{inlet}}$.

To allow for the simulation to predict the flow split between overflow and underflow, pressure boundary conditions were chosen at both outlets. Hence, atmospheric pressure was set at the hydrocyclone outlets. Air was chosen as backflow if the calculated outlet pressures fell below the atmospheric pressure.

**C. The Particle Tracking**

After calculating the flow field, the chosen microorganisms or mammalian cells were introduced. FLUENT can simulate a discrete phase in a Lagrangian formulation and, as the trajectory of any particle is computed, the program keeps track of the momentum exchange between the particle and the surrounding continuous phase. After calculating the trajectories of many particles, the resulting momentum exchange terms were incorporated in a subsequent continuous phase calculation. By alternating calculations of the continuous phase and discrete phase flows, a converged solution for the two-way coupled multi-phase flow could be achieved. The trajectories of the discrete phase were calculated using the following equation of motion for a single particle:

$$\frac{dv_i}{dt} = F_D\left(U_i - v_i\right) + \frac{\left(\rho_s - \rho\right)}{\rho_s} g_i + F_i \ , \qquad (23)$$

where $v$ is the particle velocity, $F_D(U_i\text{-}v_i)$ is the drag force per unit particle mass ($F_D$ is given by Eqn. 24), and $F_i$ are other forces acting on the particle, such as lift and Brownian forces ($F_i$ was assumed to be negligible in the present work).

$$F_D = \frac{3\mu}{\rho_s d^2} \frac{C_D}{4} \left(\frac{d\left|U - v\right|\rho}{\mu}\right) , \qquad (24)$$

where $C_D$ is the drag coefficient (evaluated through the use of the equation proposed by Haider and Levenspiel, 1989), and the term between brackets is the Reynolds number for the particle.

**D. The Efficiency Assessment**

The ultimate aim of simulating hydrocyclones is to predict their performance, i.e. to predict the total efficiency $E_T$, the reduced total efficiency $E'_T$, the reduced grade efficiency $G'$, and the reduced cut size $d'_{50}$.

The total efficiency $E_T$ is defined as the mass fraction of solids recovered in the underflow. The fraction of fluid that is discharged in the underflow is called flow ratio $R_f$. Since the fluid carries solid particles with it, some particles will be discharged into the underflow not due to the centrifugal action of the separator but due to bare entrainment. In spite of some controversy (Frachon and Cilliers, 1999; Nageswararao, 2000; Coelho and Medronho, 2001), this bypass is normally assumed to be equal to the flow ratio. Therefore, $R_f$ is the minimal efficiency at which a separator will operate even if no centrifugal action takes place.

The reduced total efficiency $E'_T$, also called centrifugal efficiency, is the separation efficiency taking into account only those particles that will be separated due to the centrifugal field. Hence, $E'_T$ does not consider the particles that are "separated" due to the flow ratio. The reduced total efficiency is defined by Eqn. (25).

$$E'_T = \frac{E_T - R_f}{1 - R_f} \ . \qquad (25)$$

The reduced grade efficiency curve $G'$ gives the centrifugal separation efficiency for each particle size present in the feed suspension. The particle size that is separated with $G'$=50% is known as the reduced cut size $d'_{50}$. $G'$ is obtained from the grade efficiency $G$, which gives the actual separation efficiency for each particle size:

$$G' = \frac{G - R_f}{1 - R_f} \ . \qquad (26)$$

The fluids used in the numerical simulations were water ($\rho$ = 998 kg m$^{-3}$ and $\mu$ = 0.001 Pa s) and air ($\rho$ = 1.225 kg m$^{-3}$ and $\mu$ = 1.79 x 10$^{-5}$ Pa s). The cells were *Escherichia coli*, *Saccharomyces cerevisiae I* (baking yeast), *Saccharomyces cerevisiae II* (brewing yeast), and mammalian cells BHK-21, whose experimental size distribution curves are given by Fig. 2. The computational code allowed the calculation of particle tracks for particles of different sizes simultaneously, and for that, the particle size distribution needed to be given as a Rosin-Rammler distribution (Rosin and Rammler, 1933).

For calculating the total efficiency $E_T$, a given mass flow rate of each of the aforementioned cells was injected into the hydrocyclone, and the particle trajectories were calculated. FLUENT could then calculate and report the mass flow rate of trapped and escaped particles, which were the particles reaching the underflow and overflow, respectively. Based on these mass flow rates, the total efficiency could be calculated. A similar procedure was adopted for grade efficiency calculations, but using mass flow rates of particles of the same size.

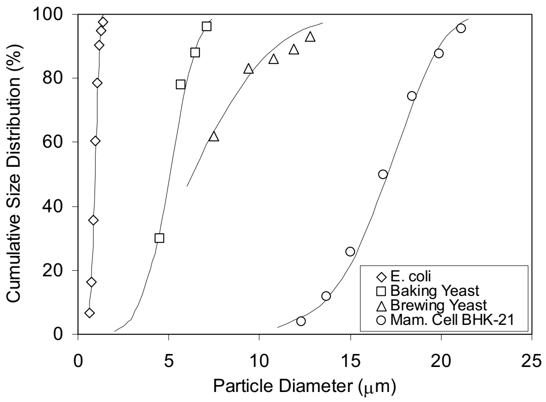


Figure 2. Size distribution (% undersize) of the cells used in the simulations.

Based on the simulated values obtained for the total efficiencies, grade efficiencies and flow ratio, the reduced total efficiencies and the reduced grade efficiencies were calculated using Eqns. (25) and (26), respectively. The reduced cut size $d'_{50}$ could then be obtained since $G'(d'_{50})=0.5$.

The workstation used for all simulations was a Compaq Alpha-server DS20, 500 MHz, 2GB RAM. The average CPU time consumed for each iteration was 4.7 s. Convergence was assumed to be reached when no further changes in the interesting quantities happened, and never before the residuals decreased to 10$^{-3}$.

## IV. RESULTS AND DISCUSSION

The numerical simulation produced a water flow ratio of 25% and a pressure drop equal to 2.1 bar, when feeding the hydrocyclone with 28 cm$^3$ s$^{-1}$ of water. For comparison, a well tested semi-empirical model (Antunes and Medronho, 1992; Castilho and Medronho, 2000) for Bradley hydrocyclones was used to predict these two variables. The results were a water flow ratio of 20% and a pressure drop of 3.3 bar. In hydrocyclones, good predictions of water flow ratios are the most difficult task. The available correlations for this purpose can lead to errors as high as 200% (Coelho and Medronho, 1992). Therefore, the 20% difference between the two water flow ratio predictions is reasonable. Empirical and semi-empirical equations correlating flow rate and pressure drop, on the other hand, produce usually good results (Antunes and Medronho, 1992; Coelho and Medronho, 1992). The lower pressure drop found in the numerical simulation is possibly due to the simplification of the feed inlet to a full 360° ring. This simplification implies that the fluid is entering the hydrocyclone in a much more smooth way.

Table 1 shows the results of total efficiency, reduced total efficiency and reduced cut size for the separation of the different cells simulated in this work. According to these results, it is not possible to separate *Escherichia coli* with the studied hydrocyclone. As Bradley hydrocyclones are high efficiency cyclones (Castilho and Medronho, 2000), it is possible to infer that bacteria can not be separated with conventional hydrocyclones down to 10 mm diameter. Yeast can be separated only with very low centrifugal efficiencies. Therefore, the use of conventional hydrocyclones to separate yeast is supposed to be unfeasible. On the other hand, an efficiency of 90% was obtained for the studied mammalian cell. This indicates that the separation of mammalian cells is an accomplishable task.

Table 1. Total efficiency ($E_T$), reduced total efficiency ($E'_T$) and reduced cut size ($d'_{50}$) obtained through Computational Fluid Dynamics (CFD), for a 10 mm Bradley hydrocyclone with an underflow diameter of 1 mm, processing 28 cm$^3$ s$^{-1}$ of a suspension of cells in water at 20°C.

| Cell | $E_T$ (%) | $E'_T$ (%) | $d'_{50}$ (μm) |
|---|---|---|---|
| Mammalian cell | 90 | 87 | 12.1 |
| Baking yeast | 46 | 28 | 8.6 |
| Brewing yeast | 28 | 4 | 11.4 |
| *E. coli* | 25 | 0 | 11.4 |

Table 2 shows a comparison between the few experimental results that can be found in the literature and the simulated results obtained in the present work. As can be seen, the experimental results confirm the fact that conventional hydrocyclones can not give high efficiencies when separating yeast suspensions.

An interesting comparison can be done based on the work of Cilliers and Harrison (1997). These authors worked with a Mozley hydrocyclone of 10 mm diameter with overflow and underflow diameters of 2 mm and 1 mm, respectively. These three dimensions are exactly the same as in the Bradley hydrocyclone simulated in this work. The authors obtained an experimental total efficiency of 27% when working with a 28 cm$^3$s$^{-1}$ of a

Table 2. A comparison between the experimental results found in the literature for separation of brewing and baking yeast with hydrocyclones and the simulated results obtained in this work.

| | This work | Cilliers & Harrison (1997) | Cilliers & Harrison (1997) | Yuan *et al.* (1996b) | Yuan *et al.* (1996a) |
|---|---|---|---|---|---|
| Yeast | Brew. & Bak. | Baking | Baking | Brew. & Bak. | Brew. & Bak. |
| Hydrocyclone | Bradley | Mozley | Mozley | Mozley & Dorr-Clone | Mozley & Dorr-Clone |
| Diameter (cm) | 10 | 10 | 10 | 10 | 10 |
| Overflow diam. (cm) | 2 | 2 | 2 | 2 & 2.6 | 2 & 2.6 |
| Underflow diam. (cm) | 1 | 1 | 1 | 2 & 1 | 2 & 1 |
| Pressure drop (bar) | 2.1 | 6.6 | 1-9 | 4 | 6 & 4.8 |
| Flow ratio (%) | 25 | - | 18 | 30-85 & 7-35 | 60 & 10 |
| Total Efficiency (%) | 28 & 46 | 22-38 | 18-33 | - | - |
| Reduced Total Eff. (%) | 4 & 28 | - | - | 10-38 & 10-15 | 36 &13 |

diluted yeast suspension. For this flow rate, the simulated total efficiency found in the present work was 28%.

A typical feature of hydrocyclones operating with the outlets opened to the atmosphere is the natural appearance of an air core, cylindrical in shape, running from the top of the overflow pipe until the underflow orifice. In the present work, an air core was formed as a result of the numerical simulation. It is important to state that no user interference, such as air bubble injection (Pericleous and Rhodes, 1986), cylinder with slip wall conditions (Averous and Fuentes, 1997) or imposition of the air core into the solution (Dai *et al.*, 1999; Dyakowsky and Wiliams, 1993) was used. The air core appeared naturally as a consequence of a low pressure region developed along the central axis during the calculations. Figure 3 shows the air core in three different sections of the hydrocyclone (see also Fig. 1 for better understanding). These three sections are the top part that includes the overflow pipe (Fig. 3.a), the central part (Fig. 3.b), and the bottom part that includes the underflow orifice (Fig. 3.c). The calculated air core had a diameter of 0.9 mm from the bottom of the vortex finder until around two thirds of the cyclone length. From the beginning of the last third part of the cyclone length until the apex, the air core started smoothly to decrease in size until it reached 0.4 mm at the underflow exit. As can be seen in Fig. 3.a, the calculated air core increased rapidly in size as it entered the overflow pipe, until it reached a stable value of 1.1 mm. The numerical calculations were also able to naturally simulate the typical shape of a spray discharge in the underflow, as can be seen in Fig. 3.c. It should be pointed out that the accuracy of the calculated size of the air core was not checked experimentally. For this purpose, a transparent hydrocyclone is being built and further investigations will be carried out.

Figure 4 shows the reduced grade efficiency as a function of the normalised diameter ($d/d'_{50}$). It can be seen that the predictions using CFD show a good agreement with the experimental points from Bradley (Bradley and Pulling, 1959) and with the curve based on experiments carried out in another work (Antunes and Medronho, 1992).

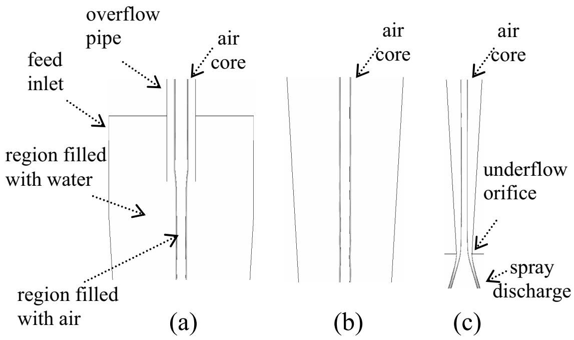


Figure 3. Details of the calculated air core for a 10 mm Bradley hydrocyclone with an underflow diameter of 1 mm, processing 28 $cm^3 s^{-1}$ of water at 20°C.

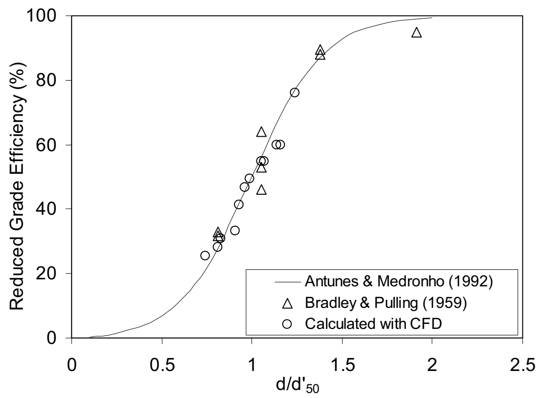


Figure 4. Reduced grade efficiency for Bradley hydrocyclones showing the predictions using CFD, the original experimental points from Bradley (Bradley and Pulling, 1959) and the curve based on experiments carried out in another work (Antunes and Medronho, 1992).

## V. CONCLUSIONS

According to CFD simulations, a 10 mm Bradley hydrocyclone can separate mammalian cells with high efficiencies. However, yeast and bacteria are not supposed to be efficiently separated by Bradley hydrocyclones, even for cyclone diameters down to 10 mm.

The computational code (FLUENT 5.1) used in the numerical simulations was capable of predicting reduced grade efficiencies curves with good accuracy.

Experiments need to be carried out to confirm the air core diameter predicted by the numerical simulations.

## NOTATION

| | |
|---|---|
| $A_\varepsilon$ | constant in Eqn. (15) |
| $A_\mu$ | constant in Eqn. (14) |
| $C_D$ | drag coefficient |
| $c_\ell$ | constant in Eqns. (14) and (15) |
| $C_u$ | Underflow volumetric concentration |
| $C_\mu$ | constant in Eqn. (12) |
| d | particle diameter (m) |
| $d'_{50}$ | reduced cut size (m) |
| $E_T$ | total efficiency |
| $E'_T$ | reduced total efficiency |
| f | fluctuating body-force per unit volume (N $m^{-3}$) |
| F | function defined in the volume of fluid model |
| $\overline{F}$ | fractional volume of the cell occupied by a given fluid |
| $F_D$ | drag force per unit of particle mass divided by $(U_i-v_i)$ ($s^{-1}$) |
| $F_i$ | other forces in Eqn. (23) (kg m $s^{-2}$) |
| g | gravity acceleration (m $s^{-2}$) |
| G | grade efficiency |
| G' | reduced grade efficiency |
| I | turbulence intensity |
| k | turbulent kinetic energy ($m^2$ $s^{-2}$) |
| $\ell$ | turbulence length scale (m) |
| $\ell_\varepsilon$ | length scale of dissipation (m) |
| $\ell_\mu$ | length scale of viscosity (m) |
| p | pressure (Pa) |
| $R_f$ | flow ratio |
| $Re_y$ | turbulent Reynolds number |
| t | time (s) |
| U | streamwise fluid velocity (m $s^{-1}$) |
| $u_i$ | $x_i$ component of fluctuating fluid velocity (m $s^{-1}$) |
| $U_i$ | $x_i$ component of mean fluid velocity (m $s^{-1}$) |
| $U_{inlet}$ | average fluid velocity at the feed inlet (m $s^{-1}$) |
| v | particle velocity (m $s^{-1}$) |
| $v_i$ | $x_i$ component of particle velocity (m $s^{-1}$) |
| $x_i$ | Cartesian direction coordinates (m) |
| y | normal distance from the wall at the cell centre (m) |
| $\varepsilon$ | dissipat. rate of turbulent kinetic energy ($m^2$ $s^{-3}$) |
| $\mu$ | liquid viscosity (Pa s) |
| $\mu_t$ | eddy viscosity (Pa s) |
| $\rho$ | liquid density (kg $m^{-3}$) |
| $\rho_s$ | solid density (kg $m^{-3}$) |
| $\Omega$ | angular rotation rate ($s^{-1}$) |

## REFERENCES


Antunes, M. and R.A. Medronho, "Bradley Hydrocyclones: Design and Performance Analysis". In: Svarovsky, L. and M.T. Thew (eds.), *Hydrocyclones: Analysis and Applications*, Kluwer, Dordrecht, Netherlands, 3-13 (1992).

Averous, J. and R. Fuentes, "Advances in the Numerical Simulation of Hydrocyclone Classification", *Can. Metall. Quart.* **36**, 309-314 (1997).

Bird, R.B., W.E. Stewart and E.N. Lightfoot, *Transport Phenomena*, John Wiley and Sons, New York (2001).

Bradley, D., *The Hydrocyclone*. Pergamon Press, London (1965).

Bradley, D. and D.J. Pulling, "Flow Patterns in the Hydraulic Cyclone and their Interpretation in Terms of Performance", *T. Inst. Chem. Eng.* **37**, 34-44 (1959)

Brayshaw, M., "A Numerical Model for the Inviscid Flow of a Fluid in a Hydrocyclone to Demonstrate the Effects of Changes in the Vorticity Function of the Flow Field on Particle Classification", *Int. J. Miner. Process.* **29**, 51-75 (1990).

Castilho, L.R. and R.A. Medronho, "Cell retention devices for suspended-cell perfusion cultures", *Adv. Biochem. Eng. Biotechnol.* **74**, 129-169 (2002).

Castilho, L.R. and R.A. Medronho, "A Simple Procedure for Design and Performance Prediction of Bradley and Rietema Hydrocyclones", *Miner. Eng.* **13**, 183-191 (2000).

Chen, H.C. and V.C. Patel, "Near-Wall Turbulence Models for Complex Flows Including Separation", *AIAA J.* **26**, 641-648 (1988).

Cilliers, J.J. and S.T.L. Harrison, "The Application of Mini-Hydrocyclones in the Concentration of Yeast Suspensions", *Chem. Eng. J.* **65**, 21-26 (1997).

Coelho, M.A.Z. and R.A. Medronho, "A Model for Performance Prediction of Hydrocyclones", *Chem. Eng. J.* **84**, 7-14 (2001).

Coelho, M.A.Z. and R.A. Medronho, "An Evaluation of the Plitt and Lynch & Rao Models for the Hydrocyclones". In: Svarovsky, L. and M.T. Thew (eds.), *Hydrocyclones: Analysis and Applications*, Kluwer, Dordrecht, Netherlands, 63-72 (1992).

Dai, G.Q., J.M. Li and W.M. Chen, "Numerical Prediction of the Liquid Flow within a Hydrocyclone", *Chem. Eng. J.* **74**, 217-233 (1999).

Dyakowsky, T. and R.A. Williams, "Modelling Turbulent Flow within a Small-Diameter Hydrocyclone", *Chem. Eng. Sci.* **48**, 1143-1152 (1993).

Fluent 5, *User's Guide*, Fluent Inc., Lebanon/USA (1998).

Frachon, M. and J.J. Cilliers, "A General Model for Hydrocyclones Partition Curves", *Chem. Eng. J.* **73**, 53-59(1999).

Haider, A. and O. Levenspiel, "Drag Coefficient and Terminal Velocity of Spherical and Nonspherical Particles", *Powder Technol.* **58**, 63-70 (1989).

Hargreaves, J.H. and R.S. Silvester, "Computational Fluid Dynamics Applied to the Analysis of Deoiling Hydrocyclone Performance", *T. Inst. Chem. Eng.* **68**, Part A, 365-383 (1990).

He, P., M. Salcudean and I.S. Gartshore, "A Numerical Simulation of Hydrocyclones", *Chem. Eng. Res. Des.* **77**, 429-441 (1999).

Hirt, C.W. and B.D. Nichols, "Volume of Fluid (VOF) Method for the Dynamics of Free Boundaries", *J. Comput. Phys.* **39**, 201-225 (1981).

Hsieh, K.T. and R.K. Rajamani, "Mathematical Model of the Hydrocyclone Based on the Physics of Fluid Flow", *AIChE J.* **37**, 735-746 (1991).

Launder, B.E., "Second-Moment Closure: Present... and Future?", *Int. J. Heat Fluid Fl.* **10**, 282-300 (1989).

Nageswararao, K., "A Critical Analysis of the Fish Hook Effect in Hydrocyclone Classifiers", *Chem. Eng. J.* **80**, 251-256 (2000).

Patankar, S.V., *Numerical Heat Transfer and Fluid Flow*, Hemisphere, Washington (1980).

Patankar, S.V. and D.B. Spalding, "A Calculation Procedure for Heat, Mass and Momentum Transfer in Three-Dimensional Parabolic Flows", *Int. J. Heat Mass Tran.* **14**, 1787-1806 (1972).

Pericleous, K.A. and N. Rhodes, "The Hydrocyclone Classifier - A Numerical Approach", *Int. J. Miner. Process.* **17**, 23-43 (1986).

Rickwood D., J. Onions, B. Bendixen. and I. Smyth, "Prospects for the Use of Hydrocyclones for Biological Separations". In: Svarovsky L. and M.T. Thew (eds.), *Hydrocyclones: Analysis and Applications*, Kluwer, Dordrecht, 109-119 (1992).

Rosin, P. and E. Rammler, "The Laws Governing the Fineness of Powdered Coal", *J. Inst. Coal* **7**, 29-36 (1933)

Vandoormaal, J.P. and G.D. Raithby, "Enhancements of the SIMPLE Method for Predicting Incompressible Fluid Flows", *Numer. Heat Trans.* **7**, 147-163 (1984).

Wolfshtein, M., "The Velocity and Temperature Distribution in One-Dimensional Flow with Turbulence Augmentation and Pressure Gradient", *Int. J. Heat Fluid Fl.* **12**, 301-318 (1969).

Yuan, H., D. Rickwood, I.C. Smyth, and M.T. Thew, "An Investigation into the Possible Use of Hydrocyclones for the Removal of Yeast from Beer", *Bioseparation* **6**, 159-163 (1996a).

Yuan H., M.T. Thew and D. Rickwood, "Separation of Yeast with Hydrocyclones". In: Claxton D., L. Svarovsky and M.T. Thew (eds.), *Hydrocyclones'96*, Mechanical Engineering Publications, London & Bury Saint Edmunds, 135-149 (1996b).

**Received: January 6, 2003.**
**Accepted: July 25, 2003.**
**Recommended by Subject Editor Leonel Teixeira Pinto.**